Materials Research Proceedings 30 (2023) 7-15 https://doi.org/10.21741/9781644902578-2

# Analysis of large deformations of long flexible bars

Artur Ganczarski[1,a*], Tomasz Gawlik[1,b]

[1]Cracow University of Technology, Jana Pawła II 37, 31-864 Kraków, Poland

[a]artur.ganczarski@pk.edu.pl, [b]t.gawlik96@gmail.com

**Keywords:** Large Deformation, Verification of Bending Test by FEM and Theory, Carbon Fibre Composite

**Abstract.** This work presents a comparison the results of the real deformation of a four-segment fly rod used to the feeder method with the results obtained from the theory and the FEM. The experiment of bending comprises preparation of the measuring path, in which the real fly rod is loaded by a series of forces subsequently changing both magnitude and inclination. The FEM model of the fly rod is based on the beam element and the variation of the cross-section is subjected to stepping approximation. The theoretical model takes advantage of the classical elliptic integral formulation applied to describe full curvature problem of long flexible bars. Dominant errors between the experimental data and numerical results come from essential difficulties in accurate measurement of the wall thickness as well as uncertainty of fibre carbon configuration.

## Introduction

Fly rods, independently of their destination, are designed as double-, triple- or four-segmental or alternatively as telescopic ones. Recently, the majority of fly rods is made of carbon fibres, whereas glass fibre fly rods represent rather lower quality goods. However, in case of many carbon fibre fly rods, where the tip segment does not play essential role in carrying of load but serves only for signalization that a fish swallows fish hook, this is so called fly rod with the vibrating tip segment, the tip segment made of glass fibre is used just for to assure sufficient stiffness.

Generally, fly rods of all kinds work in elastic range, where large bending is dominant state, whereas torsion or shear effects are negligible. Bending fly rods subjected to large deformations ought to exhibit high strength as well elasticity range. Moreover, the good quality fly rods should deform following special scheme: the deformation of tip segment resembles approximately parabola which extends towards hand grip segment according to an increasing load, and in case of advanced deformations may exhibit straightening effect.

Fly rods usually dedicated for feeder method of fishing are from 2.7m to 4.0m in length and serve for throw a masses from several grams to even 250g. The most frequent lengths of such rods are equal to 3.3m, 3.6m and 3.9m.

From the structure theory point of view, the most essential problem consists in description of fly rod deformation under loading. In case when the fly rod is treated as beam/rod element, an adequate description of deformation requires: consideration of nonlinear formula for finite curvature and simultaneously lack of prismatic shape of segments, as well as nature of loading, which may change both magnitude and direction. Associated problems known in literature of structural mechanics are as follows: finite displacements of beams – see [4], post-critical compression of column – see [5] and bending of beam of finite curvature subjected to an inclined force – see [1]. In all cases solutions are expressed by elliptic integrals and deal with prismatic beam element under concentrated load, which direction stays fixed in the space (force directed to a pole). Fundamental difficulty in adaptation aforementioned solutions to analysis of rod deformation consists in lack of prismatic shape of fly rod segments, which turn out to be conical. As consequence, engineer designing fly rod has at least two approaches to the problem: either to treat fly rod as beam/rod of step like cross-section – see section on nonlinear theory of bending, or

to take advantage of one of commercial Finite Element packages – see ANSYS Workbench model presented in further section.

**Experimental Investigations**

Test stand, shown in Fig. 1, comprises a stand supporting the fly rod, inclined to the ground with 60°, and a stand with grip to attach of a cable pulley, serving to thread a fishing line. White rope determines horizontal line necessary for setting up position of the cable pulley. Markers located subsequently at 2, 4, 6, 8 and 11m away form a hand grip of fly rod are fixed by use of a measuring tape. Both the stand of fly rod and the stand of cable pulley are made of an oak wood elements joined by steel L profiles. Loading is realized by series of normalized weights 100, 200, 500 and 1000g.

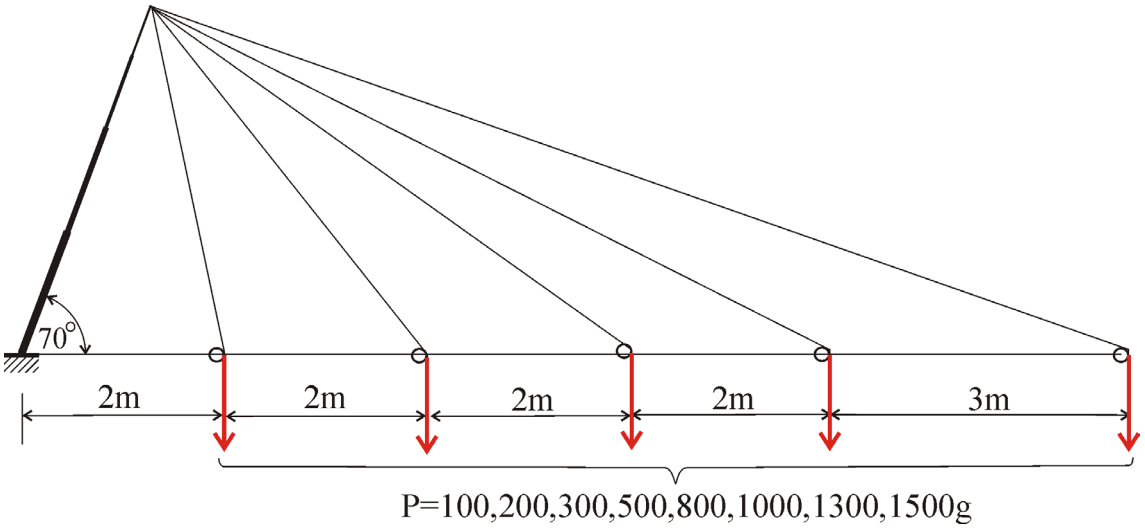


*Fig. 1. Scheme of test stand*

Experiment consists in registration by camera series of fly rod deformations referring to different combinations of load magnitude and distance measured with regard to the hand grip.

Initial test assumes following parameters: distance equal to 1.0 m, series of loading 100, 200, 300, 500, 800, 1000, 1300, 1500g and angle of inclination with respect to the ground equal 70°. This reflects final phase of towing when a fish is situated almost at the fisherman foot. Unfortunately, this test can be done for maximum weight 800g, since weight 1000g leads to failure of the fly rod. Aforementioned, negative result of initial test gives hints to the proper test characterized by following parameters: magnitude of angle of inclination with respect to the ground is decreased to 60°, minimal distance is increased to 2.0m.

Series of fly rod deformations under selected load magnitudes equal to 500, 1000 and 1500g referring to subsequent distances 11, 8, 6, 4 and 2 m are presented in Fig. 2.

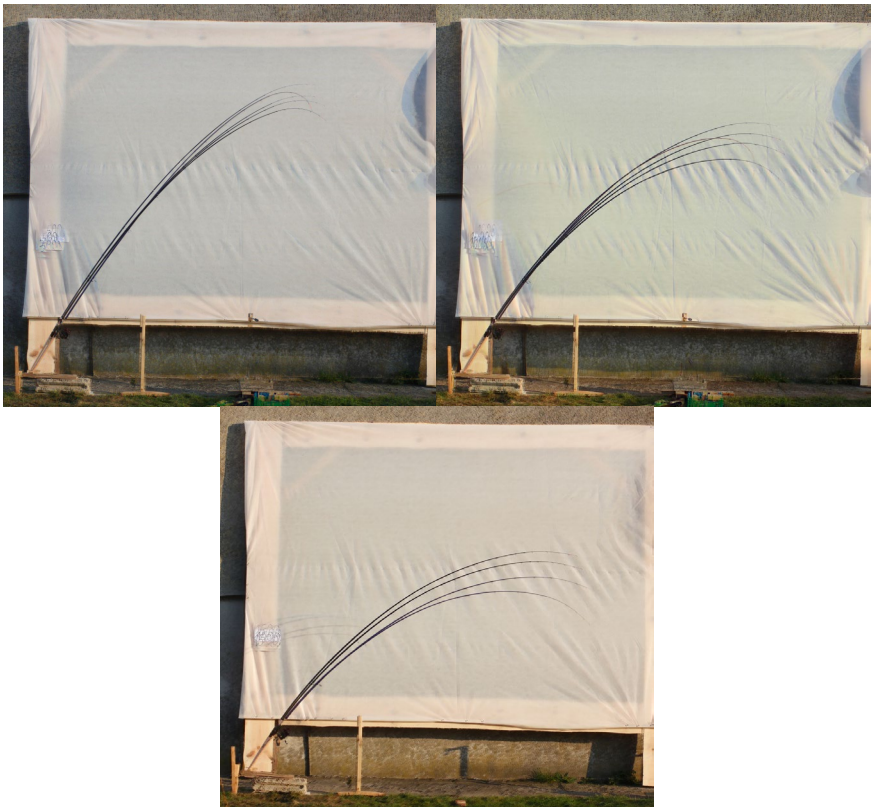

*Fig. 2. Bending test of fly rod for selected load magnitudes equal to 500, 1000 and 1500g*

**Nonlinear Theory of Bending**

Below the approach taken from monograph [1] for four-segment cantilever beam of step-like constant stiffness under concentrated force is presented – see Fig. 3.

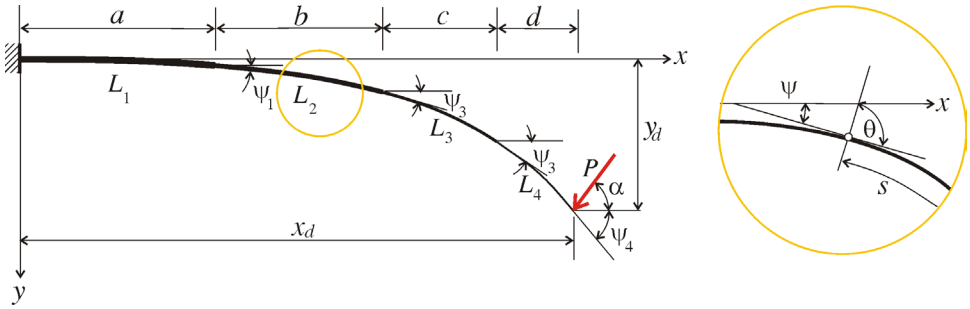


*Fig. 3. Scheme of four-segment cantilever beam of step-like constant stiffness*

Format of differential equation including magnitude of bending moment in current point (x,y) is following

$$EI_i \frac{d\psi}{ds} = M = P_1(x_d - x) + P_2(y_d - y), \quad (1)$$

where $P_1 = P \sin\alpha$ and $P_2 = P \cos\alpha$ are projections of force P according to subsequent axes, $EI_i$ denotes bending stiffness of i-th segment, whereas s stands for coordinate measured along the arc – see window in Fig. 3. After differentiation with respect to s

$$EI_i \frac{d^2\psi}{ds^2} = -P_1 \cos\psi - P_2 \sin\psi, \quad (2)$$

and introducing new variables

$$u = s/L, \quad \theta = \psi + \alpha, \tag{3}$$

one can get

$$\frac{d\theta}{du} = L\frac{d\psi}{ds}, \quad \frac{d^2\theta}{du^2}\frac{d}{du}\left(\frac{d\psi}{ds}\right)L = \frac{d}{ds}\left(\frac{d\psi}{ds}\right)L\frac{ds}{du} = \frac{d^2\psi}{ds^2}L^2, \quad \frac{d^2\psi}{ds^2} = \frac{1}{L^2}. \tag{4}$$

The right hand side of Eq. (2) can be rewritten as

$$P\left(\frac{P_1}{P}\cos\psi + \frac{P_2}{P}\sin\psi\right) = P(\sin\alpha\cos\psi + \cos\alpha\sin\psi) = P\sin(\psi+\alpha) = P\sin\theta, \tag{5}$$

whereas equation (2) itself takes format

$$\frac{d^2\theta}{du^2} + c_i\sin\theta = 0, \tag{6}$$

where $c_i = \frac{L^2 p}{EI_i} = L^2 k_i^2$. It is essential to emphasize here, that Eq. (6) is in fact the system of 4 nonlinear differential equations of second rank, which requires 8 conditions: 2 boundary conditions $+ 3 \times 2 = 6$ continuity conditions. Integration starts from 4-th tip segment using boundary condition

$$\psi(s=0) = 0 \quad \text{and} \quad \left.\frac{d\psi}{ds}\right|_{s=0} = 0 \qquad \text{or} \qquad \theta(u=0) = \alpha \quad \text{and} \quad \left.\frac{d\theta}{du}\right|_{\theta=\psi_4+\alpha} = 0, \tag{7}$$

next multiplication of Eq. (6) for $i=4$ by $2d\theta$ and integration using boundary condition Eq. (7) yields

$$\frac{d\theta}{du} = \sqrt{2c_4[\cos\theta - \cos(\psi_4+\alpha)]}. \tag{8}$$

First of Eq. (3) yields

$$du = \frac{ds}{L} = \frac{d\theta}{\sqrt{2c_4[\cos\theta - \cos(\psi_4+\alpha)]}}, \tag{9}$$

hence integration with respect to $ds$ from $\theta = \alpha$ to $\theta = \psi_3 + \alpha$ gives

$$L_4 = \int_\alpha^{\psi_3+\alpha} ds = \frac{L}{\sqrt{2c_4}}\int_\alpha^{\psi_3+\alpha}\frac{d\theta}{\sqrt{\cos\theta - \cos(\psi_4+\alpha)}}, \tag{10}$$

or in equivalent format

$$\frac{L_4}{L} = \frac{1}{\sqrt{2c_4}}\left[-\int_0^\alpha \frac{d\theta}{\sqrt{\cos\theta - \cos(\psi_4+\alpha)}} + \int_0^{\psi_3+\alpha}\frac{d\theta}{\sqrt{\cos\theta - \cos(\psi_4+\alpha)}}\right]. \tag{11}$$

Since $\cos x = 1 - 2\sin^2\frac{x}{2}$, therefore Eq. (11) can be written down as sum of two elliptical integrals of first kind

$$L_4 = \frac{1}{k_4}[\mathbf{F}(p_4) - \mathbf{F}(p_4, m_4)], \tag{12}$$

where $m_4=\sin^{-1}\left(\frac{1}{p_4}\sin\frac{\alpha}{2}\right)$ and $\sqrt{c_4}=Lk_4$.

In analogous manner, solutions for segment 3, 2 and 1 get format

$$L_i=\frac{1}{k_i}[\mathbf{F}(p_i,\zeta_i)-\mathbf{F}(p_i,\zeta_{i-1})]\,, \tag{13}$$

where $\sin\zeta_{i-1}=\frac{1}{p_i\sqrt{2}}$ and $\sin\zeta_i=\frac{1}{p_i}\sqrt{\frac{1+\sin(\psi_i+\alpha)}{2}}$.

It is convenient to compare number of equations and unknowns. There are 4 nonlinear equations (6) involving 5 unknowns $(\psi_4, p_4, p_3, p_2, p_1)$, hence numerical procedure has to be preceded by trial/error estimation of $\psi_4$. When magnitudes of $(\psi_4, p_4, p_3, p_2, p_1)$ are known next components of displacement vector can be calculated for each segment. Below solution for segment 4 (tip segment) is only demonstrated.

The infinitesimal length of arc according to Eq. (9) takes format

$$ds=\frac{d\phi}{k_4\sqrt{1-p_4^2\sin^2\phi}}\,, \tag{15}$$

and after integration we get solution being the product of trigonometric functions and elliptical integrals of first and second kind

$$x=\frac{\cos\alpha[\mathbf{F}(p_4,m_4)-\mathbf{F}(p_4,n_4)+2\mathbf{E}(p_4,n_4)-2\mathbf{E}(p_4,m_4)]+2p_4\sin\alpha(\cos m_4-\cos n_4)}{k_4}, \tag{16}$$

where $n_4=\sin^{-1}\left(\frac{1}{p_4}\sin\frac{\psi+\alpha}{2}\right)$.

In similar way

$$dy=ds\cos\psi=ds\sin(\theta-\alpha)=\frac{\cos\alpha}{k_4}2p_4\sin\phi\,d\phi-\frac{\sin\alpha}{k_4}\left(\frac{d\phi}{\sqrt{1-p_4^2\sin^2\phi}}-\frac{2p_4^2\sin^2\phi\,d\phi}{\sqrt{1-p_4^2\sin^2\phi}}\right), \tag{17}$$

finally leading to

$$y=\frac{2p_4\cos\alpha(\cos m_4-\cos n_4)-\sin\alpha[\mathbf{F}(p_4,m_4)-\mathbf{F}(p_4,n_4)+2\mathbf{E}(p_4,n_4)-2\mathbf{E}(p_4,m_4)]}{k_4}. \tag{18}$$

To end this section authors invoke basic description of elliptical integrals taken from monograph [2]. Elliptical integral of first kind in Legendre's format is the function of variable $\phi$ and parameter p as follows

$$\mathbf{F}(p,\phi)=\int_0^{\phi}\frac{d\vartheta}{\sqrt{1-p^2\sin^2\vartheta}}=\int_0^{\sin\phi}\frac{dt}{\sqrt{(1-t^2)(1-p^2t^2)}} \tag{19}$$

whereas elliptical integral of second kind in Legendre's format is the function

$$\mathbf{E}(p,\phi)=\int_0^{\phi}\sqrt{1-p^2\sin^2\vartheta}\,d\vartheta=\int_0^{\sin\phi}\sqrt{\frac{1-p^2t^2}{1-t^2}}\,dt \tag{20}$$

where parameter p is called modulus of elliptical integral. Functions $\mathbf{F}(p, \phi)$ and $\mathbf{E}(p, \phi)$ are presented in tables and for real arguments p and $\sin\phi$ are subject to change in range between 0 and 1. Complete elliptical integrals of first or second kind are functions $\mathbf{K}(p)$ or $\mathbf{E}(p)$ of modulus p and variable $\phi=\pi/2$

$$\mathbf{K}(p)=\mathbf{F}(p,\pi/2),\ \mathbf{E}(p)=\mathbf{E}(p,\pi/2)\ . \tag{21}$$

Elliptical integrals of first and second kind have closed format only for $p=0$ and $p=1$, whereas in all other cases their values are calculated by expanding in appropriate series – see [3].

**FEM Verification**

The FEM model of the fly rod is based on the beam element and the variation of the cross section is subjected to stepping approximation – Fig. 4.

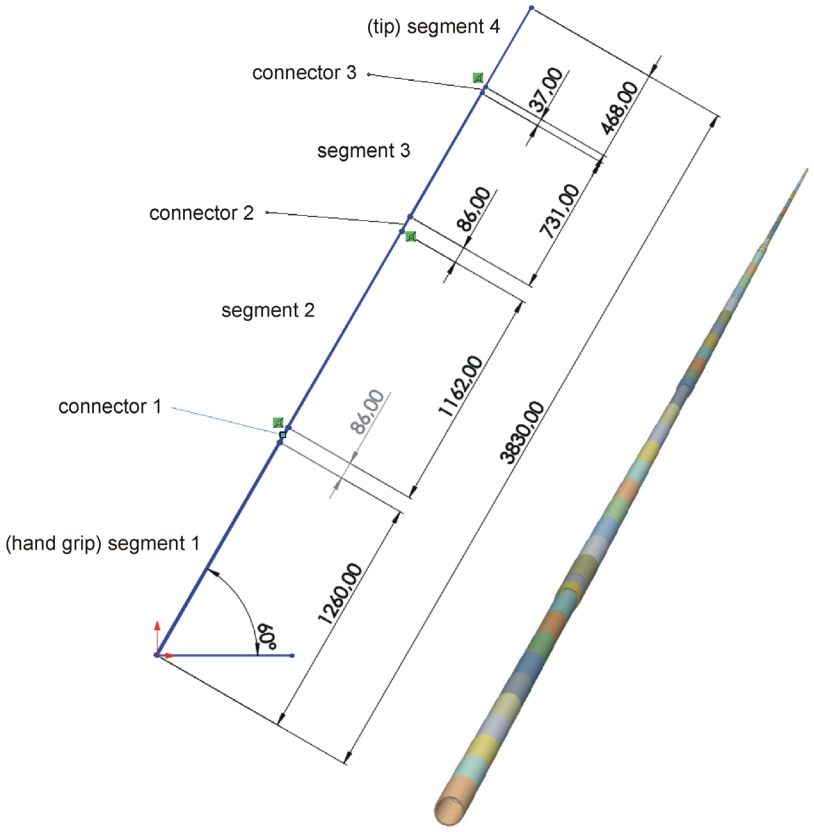


*Fig. 4. Length of subsequent fly rod elements and its FE discretization*

This approximation is based on division of each segment into ten equal elements and each connector, in which these segments link one to another, into two elements – Fig. 4.

Basic dimensions of the fly rod along perpendicular direction are small when compare to the length, hence for clearness they are collected in Tab. 1, where subsequent symbols stand for: l – length of segment, b – thickness, $D_{max}/d_{max}$ – outer/inner diameter the biggest element in section, $D_{min}/d_{min}$ – outer/inner diameter the smallest element in section, and additionally D/d – jump in diameter between two adjacent segments.

*Tab. 1. Basic dimensions of fly rod elements in [mm]*

| element | number of elements | l | b | $D_{max}$ | $d_{max}$ | $D_{min}$ | $d_{min}$ | D/d |
|---|---|---|---|---|---|---|---|---|
| segment 1 | 10 | 126 | 1.2 | 19.2 | 16.8 | 14.24 | 11.84 | 0.63 |
| segment 2 | 10 | 116 | 0.9 | 15.7 | 13.9 | 8.44 | 6.64 | 0.81 |
| segment 3 | 10 | 73.1 | 0.75 | 9.4 | 7.9 | 5.22 | 3.9 | 0.46 |
| segment4 | 10 | 46.8 | – | 3.5 | – | 1.6 | – | 0.21 |
| connector1 | 2 | 43 | 2.1 | 16.04 | 11.84 | 15.7 | 11.5 | 0.34 |
| connector2 | 2 | 43 | 1.65 | 9.94 | 6.64 | 9.4 | 6.1 | 0.54 |
| connector3 | 2 | 18.5 | – | 5.22 | – | 5 | – | 0.22 |

Finite Element package ANSYS Workbench requires definition of material model, therefore the material Epoxy Carbon UD (230 GPA) is chosen from ANSYS library as the representative of carbon fibre/epoxy resin composite. Additionally, in order to improve material properties of aforementioned composite, the data presented in Tab. 2 is taken from the website of the producer of carbon fibre composite IM7 – see [7].

*Tab. 2. Mechanical properties of carbon fibre composite IM7 [7]*

| typical hexplay 8552 composite properties (at room temperature) | US units | SI units | test method |
|---|---|---|---|
| 0°tensile strength | 395 [ksi] | 2.723 [MPa] | ASTM D3039 |
| 0°tensile modulus | 23.8 [Msi] | 164 [GPa] | |
| 0° tensile strain | 1.6 [%] | 1.6 [%] | |
| 0° flexural strength | 270 [ksi] | 1.862 [MPa] | ASTM D790 |
| 0° flexural modulus | 22.0 [Msi] | 152 [GPa] | |
| 0° short beam shear strength | 18.5 [ksi] | 128 [MPa] | ASTM D2344 |
| 0° compressive strength | 245 [ksi] | 1.689 [MPa] | ASTM Mod. D695 |
| 0° compressive modulus | 21.7 [Msi] | 150 [GPa] | |
| 0° open hole tensile strength | 62.1 [ksi] | 428 [MPa] | ASTM D5766 |
| 0° open hole compressive strength | 48.9 [ksi] | 337 [MPa] | ASTM D6484 |
| 90° tensile strength | 9.3 [ksi] | 64.1 [MPa] | ASTM D3039 |
| fibre volume | 60 [%] | 60 [%] | |

Boundary conditions applied to FE model are as follows: (hand grip) segment 1 is fully clamped at the node referring to the origin of coordinate system, whereas (tip) segment 4 load by concentrated force at the final node.

Beam elements, shown in Fig. 4 (each colour refers to separate element), are conventional iso-parametric elements – see [6], whereas mesh size is set up as default. Numerical tests with manual remeshing confirm good convergence of FE code. In order to proper capture of large deformations the Automatic Load Displacement Control (ALDC) procedure is switched on.

Numerical simulations by FEM for selected loads 500, 1000 and 1500g and variable magnitude of distance are shown in Fig. 5.

Comparison of selected experimental results and corresponding FEM and theoretical results (see Fig. 6) is done by use of commercial software tool Kinovea dedicated to image analysis. Briefly speaking Kinovea creates system of reference lines attached to photos (experiment) as well as to figures (FEM), and as a consequence it allows user for correlation of results. In general, the attained correlation is good provided that if deformation is moderate, which means referring to small magnitudes of load (100–500g) and simultaneously long distances (11–6m).

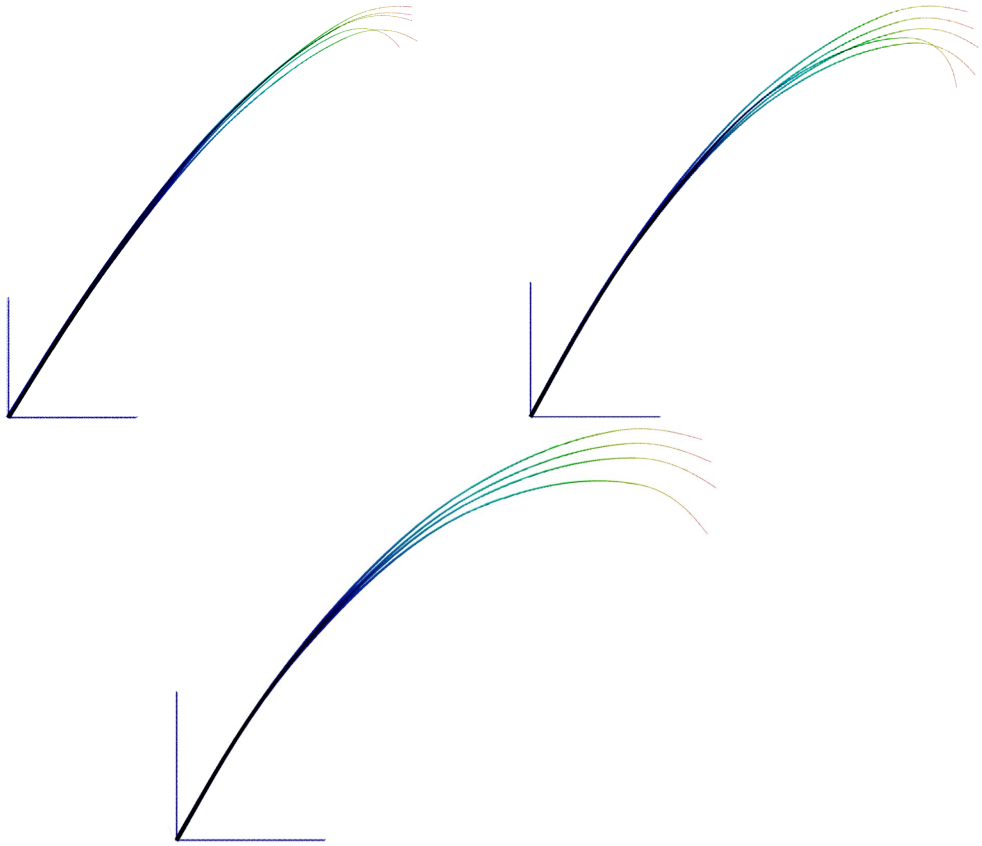

*Fig. 5. FEM results for load magnitudes 500, 1000 and 1500g*

On the contrary, in case of advanced deformations, referring to bigger magnitudes of load (800–1000g) and short distances (4–2m) some discrepancies are noticeable. Namely, central segments (#2 and #3) exhibit the biggest discrepancies for weight 1500g and distance 4m, whereas the tip element (#4) is responsible for generation of main discrepancies for weight 1000g and distance 2m.

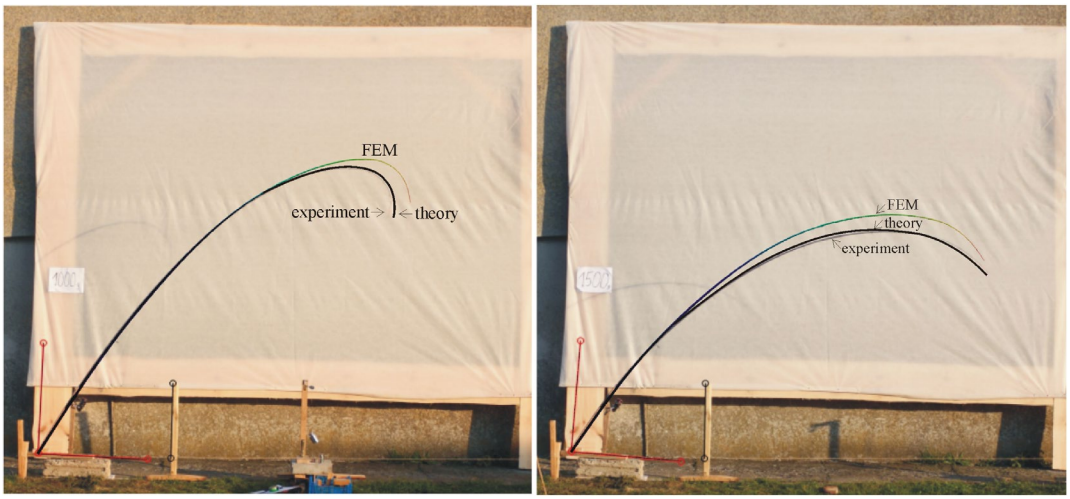


*Fig. 6. Comparison of experimental, FEM and theoretical results for two selected combinations of load magnitudes and distances*

In the opinion of authors of present work, there are two main sources of discrepancies:

- lack of information about the wall thickness, particularly with regard to central segments, that may essentially influence their stiffness,
- lack of honest information concerning carbon fibre configuration in the composite thus authors assumes orientation $0^o$–$90^o$ as a default.

## Conclusions

Presented experimental data is well mapped by numerical results in case of moderate deformations, whereas major discrepancies observed for advanced deformations come from:

- essential difficulties in accurate measurement of the wall thickness,
- uncertainty of fibre carbon configuration, that is subject to commercial confidentiality.

Additionally, in case when even ALDC procedure (built in FEM package) fails the nonlinear theory of bending, taking advantage of elliptical integrals, is recommended for use.

## References

[1] R. Frisch-Fay, Flexible bars, London Buttherworths, 1962.

[2] F. Oberhettinger, W. Magnus, Anwendung der Elliptischen Funktionen in Physik und Technik, Springer-Verlag, Berlin-Heidelberg, 1949. https://doi.org/10.1007/978-3-642-52793-7

[3] W. Press, S. Teukolsky, W. Vetterling, B. Flanner, Numerical Recipes in Fortran 77: The Art of Scientific Computing, Cambridge University Press, NY, 1997.

[4] S.P. Timoshenko, J.M. Gere, Mechanics of materials, Van Nostrand, New York, 1972.

[5] M. Życzkowski, Pokrytyczne zachowanie się prętów ściskanych, in: Mechanika techniczna, vol. IX, PWN, Warszawa, 1988, pp. 298–304.

[6] Information on http://riad.usk.pk.edu.pl/~m1/mysql/materialydydaktyczne/pliki/lkpizimes1.pdf

[7] Information on https://www.hexcel.com/user_area/content_media/raw/IM7_HexTow_Data Sheet.pdf